Molecular Understanding of Nitrogen Oxide Fixation of Water-Lean Carbon Capture Solvents by Atomistic Modeling

Loukas Kollias,[a] Manh-Thuong Nguyen,[a] Sarah I Allec,[a] Deepika Malhotra,[a] Difan Zhang,[a] Roger Rousseau,[b] Vassiliki-Alexandra Glezakou,[b] Phillip K Koech,[a] and David J Heldebrant[a,c]*

a. Pacific Northwest National Laboratory, Richland, WA 99352, United States

b. Oak Ridge National Laboratory, Oak Ridge, TN 37831, United States

c. Washington State University, Department of Chemical Engineering, Pullman, WA 99164 United States

KEYWORDS: CO_2 capture solvent, Fixation, Atomistic modeling, Water-lean solvents, Nitrogen oxides.

ABSTRACT

Nitrogen oxides, present in flue gas, can cause negative impacts on amine carbon capture solvents by the formation of heat-stable salts and suspected carcinogens. Thus, to maximize the performance of water-lean solvents, a better understanding of this process in these systems is necessary. Here, a computational study for the fixation of the CO_2 capture solvent N-(2-ethoxyethyl)-3-morpholinopropan-1-amine (EEMPA) to nitramine/nitrosamine was conducted. The first step involves the dissociation of the NH bond of EEMPA, in which the homolytic mechanism, is energetically more favorable than the heterolytic mechanism. The second step involves radical recombination to form N-N bonds. While NO_2 directly reacts with EEMPA, NO has almost no effect. However, in the presence of O_2, fixation of EEMPA by NO is enhanced via the formation of N_2O_4 species. Low reaction energies indicate that the formation of nitramine/nitrosamine may be a reversible process, suggesting that EEMPA could be recovered under thermal stripping conditions.

1. Introduction

Carbon dioxide (CO_2) is one of the main contributors to greenhouse gas emissions to the atmosphere. Accumulation of these emissions contributes to the greenhouse effect that is related to increasing global temperatures.[1] Consequently, CO_2 capture is key to mitigating the dire

consequences of this effect. Amine-based solvents are ordinarily used to capture CO_2 from either industrial flue gas streams (point-source capture) or directly from the air (direct air capture).[2, 3] Recently, there have been efforts to optimize the performance, lifetime, and manufacturing and maintenance costs of carbon capture solvent systems.[3]

Water-lean solvents were introduced to alleviate the costs associated with the regeneration of aqueous amines.[3] Nevertheless, these amines are still susceptible to thermal and oxidative degradation as well as fixation due to interactions with nitrogen and sulfur oxides, NO_x and SO_x (x=1,2), present in the flue gas.[4, 5] Fixation limits the lifetime of these post-combustion CO_2 capture solvents and induces corrosion. As a result, operating costs related to solvent replacement and equipment maintenance are increased.[6-9] Also, there is environmental concern due to pollutants emitted as a result of amine fixation.[8, 10]

Common mechanisms of amine fixation are due to thermal, oxidative, and hydrolytic deterioration. Thermal fixation is induced by carbamate polymerization at high temperatures (> 100 ^oC) in the stripping column.[5, 8, 11] Additionally, oxidative fixation occurs due to interactions between the amine and O_2 producing aldehydes and carboxylic acids. [8, 9, 12] Furthermore, amines degrade due to interactions with NO_x and SO_X impurities in the gas stream[5] both at the carbon capture unit as well as in the atmosphere.[5, 13] Reactions of amines with SO_x, NO_x produce heat-stable salts that lower the CO_2 capacity of the amine, while NO_x leads to toxic and carcinogenic by-products. [5, 14] Furthermore, SO_x, NO_x capture by the amine competes with CO_2 capture; hence it reduces the efficiency of the latter.[15]

NO_x molecules are irreversibly absorbed in the solvent making a heat-stable salt (HSS); hence inducing deactivation.[16-18] NO_x in the flue gas stream consists mainly of nitrogen monoxide (NO) and then nitrogen dioxide (NO_2). Typical concentrations after flue gas desulfurization and selective

catalytic reduction are ~ 200 ppm for NO and ~ 20 ppm for NO_2.[19] Nevertheless, NO_2 has higher affinity to amine-based solvents due to its higher acidity and polarity compared to NO that is much less reactive with amines.[17] Reactions between amines and NO_2 in the absorber and nitrite (NO_2^-) in the desorber unit results in the release of toxic pollutants such as nitramines and nitrosamines.[8, 17, 20] Primary amines are less prone to nitrosation than secondary and tertiary amines[21] but they can degrade to secondary amines in the presence of NO_x which further degrade to nitrosamines after reacting with NO_2.[11, 18, 22, 23] Nitramines and nitrosamines attract significant interest as they are harmful to the environment and suspected carcinogens.[14, 20, 22, 24, 25] Amine nitrosation is faster than nitration in the CO_2 capture unit; hence studies have focused on its inhibition.[14] The nitrosating and nitrating agents, N_2O_3 and N_2O_4, react with amines to produce N-nitrosamines and N-nitramines respectively.[26]

Huang et al. [7] found that the formation of nitrite can considerably fixate monoethanolamine (MEA), a well-known carbon capture solvent. Wang et al. [27] postulated that solvent fixation depends both on the reaction pathway, conditions, and composition of the solvent mixture,[28] concluded that free radical NO_2 absorption dominates total NO_x absorption at ppm levels of nitrogen oxides[29] suggested that reactions with nitrite fixate amines possibly through forming short-lived primary N-nitrosamine intermediates.

Static calculations at the density functional theory (DFT) level have been used to study amines reacting with NO_x gases.[25] Zhao et al. [30] suggest that a reaction mechanism involving the formation of free radical species during nitrosation of secondary amines occurs in the presence of NO_x. Sun et al. [31] studied the structure reactivity relationship of amines in N-nitrosation reactions. They found that heterocyclic amines, like the one we select to study in this work, have the highest reactivities and that the value of the pyramidalization angle is proportional to reactivity. Liu et al.

[32] found three possible pathways for the reaction of a N-nitrosodimethylamine (NDMA) with nitrite catalyzed by heavy metals concluding that Cd^{2+} accelerates nitrosation. Liu et al. [33] concluded that reactive nitrogen species play a key role toward the nitrosation of NDMA, while Lui et al. [34] found that nitrosation is more favorable than nitration of dimethylamine (DMA). They later studied further reaction between DMA and nitrite to form NDMA[35] in a multiple-step reaction, where the rate-determining step is the nucleophilic addition of DMA with carbonyl compounds. At last, Lv et al. [36] found that the formation of nitrosamines from ethylamino and diethylamino radicals reacting with NO is a highly exothermic process. Recently, Lv et al. [37] studied the fixation of DMA to nitramine and nitrosamine using both *in situ* spectroscopic methods and static DFT calculations. The reaction involves a hydrogen-bonded intermediate and the subsequent formation of an aminyl radical.[37] Also, N_2O_4 and N_2O_3 react with DMA to form nitramine and nitrosamine.[37] Yu et al. [38] studied piperazine nitrosation using quantum chemistry calculations. They found that CO_2 accelerates piperazine fixation due to the formation of $ONOCO_2^-$ from its reaction with nitrite. These examples show that quantum chemistry and DFT calculations for gas-phase systems have been mainly used to understand amine fixation by NO_x. However, in practice, fixation of CO_2 capture solvents occurs in liquid phase. Thus, in modelling studies, full solvent boxes help describe realistic systems.

In this work, we use a variety of computational chemistry methods to study these systems including (1) static DFT calculations to energetically assess the possible reaction paths and guide condensed phase calculations, (2) classical molecular dynamics (CMD) to calculate solvent density, and (3) ab initio molecular dynamics (AIMD) to evaluate reactivity and obtain a mechanistic understanding of solvent fixation due to impurities that are present in the flue gas stream. We focused on N-(2-ethoxyethyl)-3-morpholinopropan-1-amine (EEMPA) fixation by

NO_x. This solvent, first synthesized by us[39], is a single-component water-lean solvent with a very low total cost of capture, $39 per tonne CO_2 [40] 13.3% cheaper than the National Energy Technology's (NETL) B12B amine baseline case.[41] At the same time, it is a highly efficient and highly durable amine-based water-lean post-combustion CO_2 capture solvent.[42, 43] Also, EEMPA can decrease CO_2 capture capital and operating costs due to its wettability that allows for cheaper materials of construction and lower energy demand, as low as 2.0 GJ per tonne CO_2 operational reboiler heat duty, for solvent regeneration, respectively,[42] 13% lower than the NETL B12B baseline case.[41]

The rest of this paper is organized as follows: In the Methods section, details of computational and experimental techniques are provided. In the Results section, reaction energetics in the gas-phase; species, energetics, solvent density, and reaction paths in the condensed phase, are presented. We will close the paper with conclusion and outlooks.

2. Methods

Depending on the chemical reaction or property under study, a combination of molecular modelling methods is often necessary to study carbon capture solvent fixation.[2] Here, we focus on the reaction of NO_x with solvent-fixated CO_2 to assess the stability of CO_2 capture solvents.

2.1. Gas-phase density functional theory calculations

Gas-phase structural optimization studies of chemical reactions guide condensed phase studies and provide initial estimate of reaction energetics for both NO and NO_2 loading. These were performed at the DFT level using the B3LYP exchange-correlation functional[44] and 6-31G** basis functions.[45] All calculations were performed using NWChem.[46]

2.2. Classical Molecular Dynamics

CMD simulations provide an initial estimate of liquid structure and density. These were performed using the GROMACS program,[47] and the all-atom OPLS force field (OPLS-AA). [48] The necessary force fields were generated using the LigParGen web server[48, 49] (http://zarbi.chem.yale.edu/ligpargen/) except from the partial atomic charges. These were calculated after fitting a quantum mechanical electrostatic potential to EEMPA, and EEMPA-NO_2 molecules, at the B3LYP/6-31G** level of theory as implemented in NWChem.[46]

We sampled configurations in the isothermal-isobaric (NPT) ensemble using the stochastic cell rescaling barostat[50] to equilibrate the solvent density. The leap-frog integrator was used with a 1 fs time step. The particle-mesh Ewald (PME) scheme was used for electrostatics. The cut-off for van der Waals and electrostatic interactions was set to 9.5 Å. Subsequently, these solvent boxes were used in AIMD simulations. Each solvent box contains 20 EEMPA molecules. Also, we prepared large simulation boxes of 200 EEMPA molecules each to calculate density at increasing temperature. Two NO_2 molecules were added to the boxes after solvent density equilibration using CMD simulations.

2.3. Ab initio molecular dynamics

To understand and quantify solution phase reactivity between NO_x and solvent, we used AIMD which employs the strength of both quantum chemistry and molecular dynamics. Born-Oppenheimer AIMD simulations were performed for condensed phase systems at the PBE-D3 density functional level.[51] Within the hybrid Gaussian – plane wave DFT scheme,[52] we used the DZVP basis sets,[53] in conjunction with a plane-wave cutoff of 450 Ry. The canonical (NVT) ensemble, in which the temperature T was kept at 310 K by the Nose-Hoover thermostat, [54] was adopted. AIMD simulations were performed using the CP2K program.[55] Geometries obtained from CMD served as the starting point for AIMD simulations. Each system was first equilibrated with

a 10 ps run, followed by a production run of 10 ps. Finally, these systems were annealed to a low temperature (< 10 K). The diffusion coefficient of NO_2 was calculated using the mean square displacement approach.

2.4. Reaction energy barrier calculations and charge analyses

To evaluate the reaction energy barrier in the condensed phase, we performed geometry optimization while constraining the bond distance (for N-H, N-N), then climbing image nudged elastic band calculations[56] for transition states. In the condensed phase these minima were determined by static optimization of frames, annealed from AIMD simulations. Atomic charges were calculated through the Bader analysis.[57]

3. Results

3.1. Gas-phase reaction energies

We explored the possible reactions of EEMPA with various reactants. Two potential solvent fixation mechanisms were considered, one through charged intermediates and one through radicals. These are consistent with the N-nitrosation of amines by NO_x from a theoretical study,[30] and the formation of nitrosamine/nitramine from NO_x reaction with amines from experiment. [58] In the first case, that is the reaction R1A in **Scheme 1**, a NH bond in EEMPA homolytically dissociates to form a radical (R_2N^*) and another product NO_xH^*. In the second case, see Reaction R1B in **Scheme 1**, a NH bond of EEMPA heterolytically dissociates resulting in ionic species, a deprotonated EEMPA (R_2N^-) and a protonated NO_x. As shown below, R1A is energetically more favorable then R1B, thus in a subsequent step, the reaction of R_2N^* with a second NO_x molecule is considered, see the reaction R2 in **Scheme 1**. It is known that the reactions of small molecules in the gas phase, for example,[59, 60] $O_2 + 2NO \rightarrow 2NO_2$, can be thermodynamically feasible and

kinetically fast, we thus also considered these reactions (R0) as a pre-fixation step. The energetics of related reactions is summarized in **Fig. 1**, in which we used the reactants as reference states.

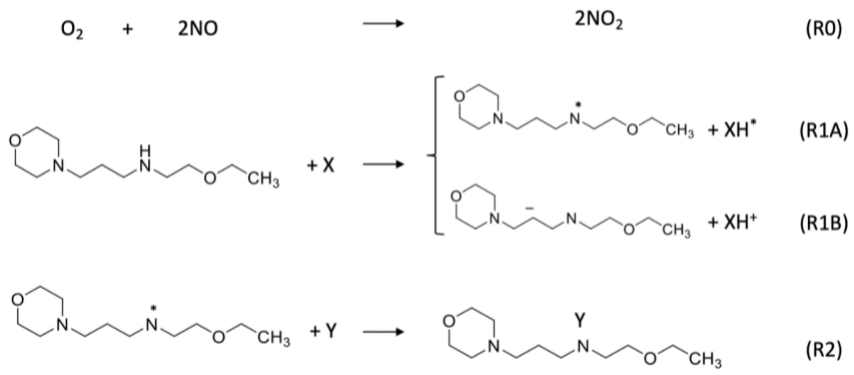

Scheme 1. Reaction mechanisms of EEMPA with X (X=NO, NO_2, O_2, H_2O, N_2O_2, N_2O_3, N_2O_4, EEMPA) and Y (Y=NO_2, NO): with radical (R1A) and anion (R1B) products. The symbol * indicates radical species. R2 shows reaction of dehydrogenated EEMPA (radical) with Y (Y=NO, NO_2). An example of the reaction between two small molecules (R0).

We start our discussion with the reaction of small molecules, R0. The reaction $2NO_2 \rightarrow N_2O_4$ is an exothermic process with an energy change of 0.65 eV, which is consistent with experimental enthalpy values 0.56-0.62 eV (54-60 kJ/mol).[60] Similarly, the energy of the NO + NO_2 → (asymmetric) N_2O_3 reaction is -0.41 eV, similar to experimental enthalpy of about -0.42 eV. [61] Our calculations predict a very small energy change for the 2NO →(cis-) N_2O_2 reaction, about 0.0 eV, consistent with the experimental enthalpy of 0.6 kJ/mol.[61] Consequently, the formation of N_2O_3 is more likely than the formation of N_2O_2 in a 50 NO: 50 NO_2 mixture. In the presence of O_2, NO can transform into N_2O_4:[59] $2NO + O_2 \rightarrow 2NO_2 \rightarrow N_2O_4$. The energy change in the first step $2NO + O_2 \rightarrow 2NO_2$ is calculated at -1.30 eV, combining with the reaction energy of $2NO_2 \rightarrow N_2O_4$, we found the energy change of -1.95 eV for $2NO + O_2 \rightarrow N_2O_4$. This suggests that O_2 can play an important role in the fixation process of EEMPA by NO. [24]

We now look at the reaction R1A. **Fig. 1** clearly shows that the stability of intermediate species R_2N^* strongly depends on the reactants. While the O_2+2NO + EEMPA (→ N_2O_4 + EEMPA) → R_2N^* + HN_2O_4 path is exothermic (reaction energy = -0.62 eV), other paths are endothermic. For NO, the reaction NO + EEMPA → R_2N^* + HNO is more endothermic than NO + NO + EEMPA → N_2O_2 + EEMPA → R_2N^* + HN_2O_2, by 0.7 eV. Therefore, the dimerization of NO is likely an elementary step in the fixation of EEMPA. For NO_2, we observed a similar trend: the dimerization of N_2O_4 is likely to involved since the reaction $2NO_2$→ N_2O_4 is highly exothermic (with the reaction energy being -0.64 eV). The intermediate (R2N* + HN_2O_4), resulting from the reaction between EEMPA and N_2O_4, has an energy of 0.69 eV *vs.* the reference energy of (EEMPA + $2NO_2$), indicating a possible reaction path. If there is no dimerization between NO_2 molecules, the reaction NO_2 + EEMPA → R_2N^* + HONO is also likely since the formation of a stable species HONO lowers the total energy of the intermediate (R_2N^* + HONO). With NO and NO_2 mixture, the formation of N_2O_3 also leads to a more stable intermediate compared to the NO + EEMPA or NO_2 + EEMPA path. The reaction O_2 + EEMPA → R_2N^* + HO_2 is a highly endothermic process (reaction energy is +2.0 eV). This suggests that O_2 does not facilitate NO degrading EEMPA by directly interacting with the solvent. In contrast, it facilitates solvent fixation by reacting with NO to form a stronger H-binding molecule, N_2O_4, that stabilizes R_2N^*. Moreover, water or EEMPA do not stabilize the intermediate as the neutral H_3O or EEMPA-H complexes, respectively, are not stable.

In the last step, the coupling between radical species R_2N^* and NO_x is expected to be exothermic. Compared to the 2NO + EEMPA reactant, the final product R_2N-NO + HNO is slightly less stable. For the ($2NO_2$ + EEMPA) reactant, the product (R_2N-NO_2 + HNO_2) is 1.2 eV more stable. For the (NO + NO2 + EEMPA) reactant, the product (R_2N-NO + HNO_2) is more stable than (R_2N-NO_2 +

HNO). For the (O_2 + NO + EEMPA) reactant, the product (R_2N-NO + HO_2) is slightly less stable. The most stable product (R_2N-NO_2 + HNO_2) is found with the reactant (O_2 + 2NO + EEMPA). The reaction energy in the latter case is -2.5 eV. See Figure 1 for stable structures of HN_xO_y.

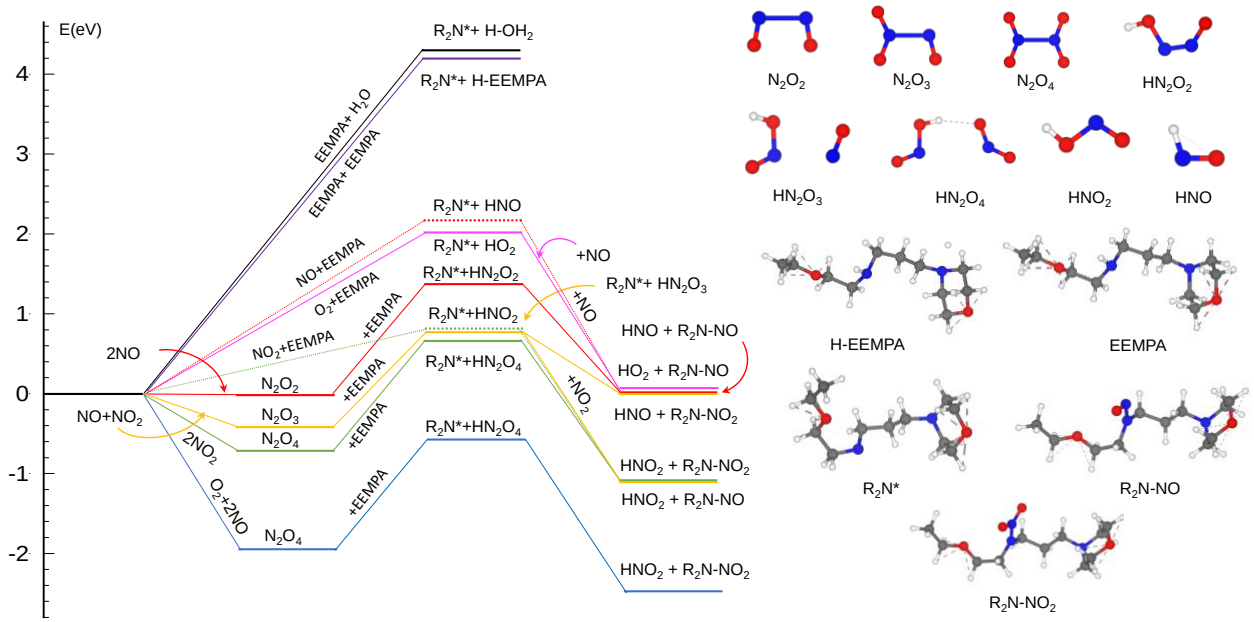

Figure 1. Reaction of gas molecules with EEMPA to form R_2N-NOx species. The reactant energy is the reference energy. Atomic structures are DFT-optimized, the N-N bond is spontaneously broken during the optimization in the HN_2O_4 and HN_2O_3 structures. Our calculations show that EEMPA is much less prone to fixation by NO than by NO_2. This finding is consistent with the fixation study of secondary amines (N-methylaminopropyl) trimethoxysilane, in which NO shows minor effects on, while NO_2 can decrease more than 90%, the CO_2 capacities of the amines. [62] However, adding NO_2 to the system enhances EEMPA fixation by NO. If the molar fraction of NO_2 is less than that of NO, then it is likely that they will form N_2O_3 (and remaining NO), HN_2O_3 stabilizes the intermediate R_2N^*, while HONO stabilizes R_2N-NO. Most strikingly, introducing O_2 to NO significantly promotes EEMPA fixation. A similar finding was reported for the

enhancement of nitro-sodiethanolamine formation in monoethanolamine by introducing O_2 to NO_x. [22]

Table 1. Energies ΔE of reactions R1B in **Scheme 1**.

X	$\Delta E(eV)$
NO	11.91
NO_2	11.22
N_2O_2	10.13
N_2O_3	9.49
H_2O	9.87
EEMPA	9.86

To close this section, we will show that the anionic mechanism (R1B, Scheme 1) is very unlikely for the fixation of EEMPA. **Table 1** shows that the reaction R1B is a highly endothermic process, (reaction energy ~10-11 eV). This is mainly due to the unstable R_2N-anion.

3.2. EEMPA solvent density

We performed CMD simulations of EEMPA in the liquid form as well as with 5 % NO_2 loading, forming R_2N-NO_2. In the first scenario, a simulation box of pure EEMPA liquid consisting of 200 molecules is equilibrated using the stochastic cell rescaling barostat.[50] In the second scenario, 5 % of the molecules in the simulation box were loaded with NO_2.

The density profile along a range of temperatures from 290 K to 370 K is compared with experimental findings. We find that the force field overestimates the density of liquid EEMPA by 3.7% compared to experiment. Systems of EEMPA loaded with NO_2 are denser at the temperature range studied in this work. Low loading with NO_2 slightly increases density. The latter increases by less than 1 % in all systems studied with a 5 % NO_2 loading. The resulting density profiles from both simulation and experiment are shown in **Fig. 2**. Detailed data from computations and experiment are available in **Table S1** in the Supporting Information, SI.

We perform linear regression to find the line of best fit for the three cases studied. This way we can calculate density as a function of temperature. Consequently, the experimental density (g/cm^3) measured for EEMPA follows,

$$\rho(T) = -0.00075000 \cdot T + 1.1818625\,, R^2\text{: } 0.998 \qquad (1)$$

the EEMPA density calculated from theory can be approximated as,

$$\rho(T) = -0.00088495 \cdot T + 1.2598355, R^2\text{: } 0.999 \qquad (2)$$

Finally, the density in the case of 95mol% EEMPA + 5mol% R_2N-NO_2 follows,

$$\rho(T) = -0.00090720 \cdot T + 1.2753260, R^2\text{: } 0.987 \qquad (3)$$

where, R^2 is the coefficient of determination. Both experimental and computational data show an almost linear dependence of the density on the temperature ($R^2 \approx 1$). The density for NO_2 containing system, equation (3), is used for AIMD simulations.

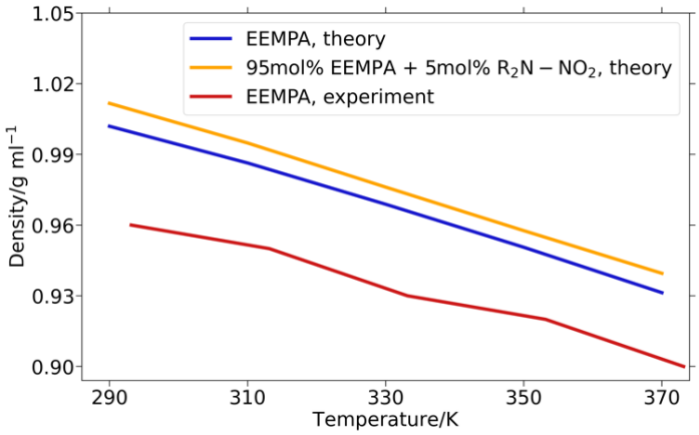

Figure 2. Density profiles of all systems used compared with experiment (solid red line). Densities calculated using charges from an electrostatic potential fit are shown with solid line plots (blue – liquid EEMPA, cyan – NO_2-loaded EEMPA).

3.3. Possible formation of the N_2O_4 species in solvent

In the condensed phase, the reaction is also found to be exothermic consistent with gas phase calculations. **Fig. 3a** shows the trajectory of a NO_2 molecule in a ~10 ps AIMD simulation. The diffusion coefficient of NO_2 is estimated at $\sim 6 \cdot 10^{-5}$ $cm^2 s^{-1}$ indicating that NO_2 is very mobile in the solvent. **Fig. 3b** shows two NO_2 molecules forming a N-N bond. The bond length is characterized by calculating the radial distribution function of the N-N atom pair, see **Fig. 3c**. The, the first peak corresponds to the equilibrium N-N bond distance in N_2O_4. This is calculated at ~1.8 Å, hence it is consistent with gas phase calculations. N_2O_4 is also found energetically more stable than two NO_2 molecules, by 0.41 eV, suggesting that NO_2 forms N_2O_4 before interacting with EEMPA.

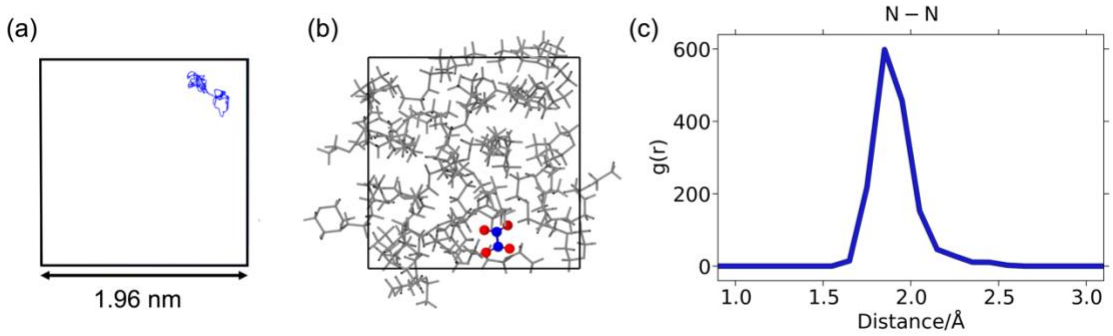

Figure 3. (a) Trajectory of a NO_2 molecule in the EEMPA solvent box (EEMPA not displayed) in a ~10 ps simulation. (b) Structure of N_2O_4. (c) radial distribution of the N-N pair of N_2O_4.

3.4. R_2N-NO_2 species in the EEMPA solvent

The goal of this section is to confirm the stability of the R_2N-NO_2 product in the solvent. In the liquid phase, the resulting H atom (from the dissociation of the NH bond of EEMPA) in principle can bind to the O atom of the -NO_2 group or the N atom in the aliphatic chain, see structures A and B in **Fig. 4**, resembling the acid and zwitterionic structures [63] of CO_2-bound EEMPA. However, the most stable structure is C, which is characterized by a H atom bound to a second NO_2 molecule resulting in the formation of the HONO species. The relative energies of these structure are also provided in **Fig. 4**. It appears that the R_2-NO_2 structure is the most stable.

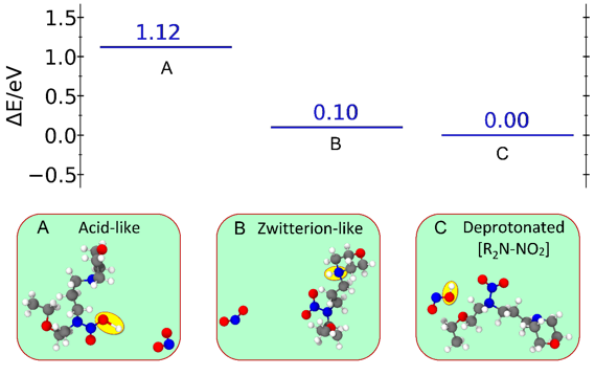

Figure 4. Different NO_2-EEMPA structures sampled in AIMD simulations and their relative energies. The O-H bond in structures A and C, and the N-H bond in structure B are shown in yellow background. For clarification, only reactant molecules are shown.

3.5.Condensed phase calculations for the reaction of N_2O_4 with EEMPA

We now investigate the two steps of the reaction N_2O_4 + EEMPA→ R_2N-NO_2 + HONO. The potential energy landscape of this process is provided in **Fig. 5**. We started from the N_2O_4 since the dimerization of NO_2 molecules is likely, and the H from the dissociation of the NH bond (H^*) interacts with NO_2, forming a stable specie HONO. As shown in **Fig. 5**, we considered two steps: the dissociation of the NH bond, resulting in the undercoordinated N atom (N^*), and the coupling between the N of NO_2 with this atom. The intermediate (N^*+ NO_2 + HONO) was obtained by performing geometry optimizations while moving the H atom of the NH bond close to N_2O_4. The reaction energy is ~1 eV, while the corresponding barrier is 1.3 eV. In the transition state of this rate-limiting step, the N-H bond of EEMPA is broken (2.1 Å) while the O-H bond (in HONO) is developed (1.0 Å). The next step is highly exothermic, with an energy change of ~ 1.3 eV. The barrier associated with this step is ~ 0.1 eV, suggesting a fast process. The total reaction energy is ~ -0.3 eV, consistent with the value of ~ -0.5 eV obtained from gas phase calculations.

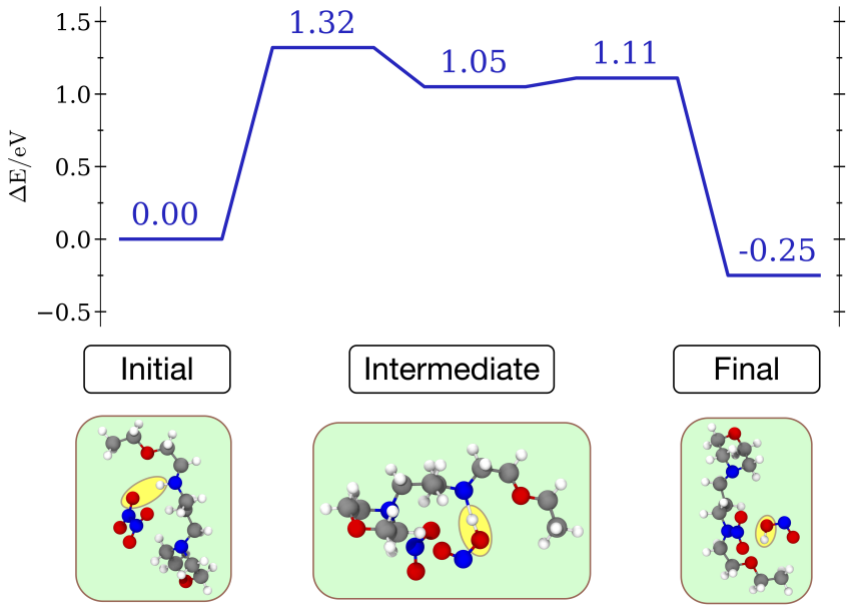

Figure 5. The energy landscape of the N_2O_4 + EEMPA → HONO + R_2N-NO_2 reaction in the solvent. The O-H interactions are shown in yellow background. For clarification, only reactant molecules are shown.

Now we look at the charge states of R_2N^*, N^*, H^*, and N_2O_4 in the initial, intermediate, and final structures. **Table 2** shows that the total charge of R_2N^* and H^* becomes more positive while that of N_2O_4 becomes more negative along the reaction pathway, as expected in the oxidative degradation. In the initial state, N_2O_4 is already reduced by -0.12 |e|. In the intermediate, the total charge of N_2O_4 (N_2O_4 in this case means a "free" NO_2 and a NO_2 binding to H^*) is -0.91 |e| which is further decreased to -1.0 |e| in the final structure. Conversely, the EEMPA molecule ($R_2N^* + H^*$) is slightly oxidized by +0.06 |e| but strongly oxidized in the final structure, by +0.92 |e|. The N^* atom becomes less negatively charged and the H^* atom becomes more passively charged along the reaction path. In the intermediate structure, the total charge of R_2N^* is 0.07 |e|, which, by charge calibration, shows that R_2N^* is a radical. This agrees with the radical mechanism obtained from

gas-phase calculations, which is shown in section 3.1 to be energetically more favorable than the anionic mechanism.

Table 2. Charge of R_2N^*, N^*, H^*, and total charge of N_2O_4 (unit |e|) in the initial, intermediate, and final states.

Structure	R_2N^*	N^*	H^*	N_2O_4
Initial	-0.32	-1.02	0.38	-0.12
Intermediate	0.07	-0.80	0.56	-0.91
Final	0.32	-0.61	0.60	-1.0

4. Conclusions

Amine-based carbon capture solvents degrade due to interactions with NO_x species which are present in both flue gas streams and the atmosphere. We focused on the reaction mechanism of a water-lean carbon capture solvent, EEMPA, that offers low-cost CO_2 capture, due to interactions with NO and NO_2.

Static DFT calculations show that fixation of NOx by EEMPA most likely involves the formation of radical species, R_2N^*, promoted by the homolytic NH bond dissociation. NO_2 has a more significant effect on the fixation of EEMPA than NO. This is further corroborated by experimental studies.[62] NO_2 molecules form N_2O_4 and N_2O_3 adducts in the presence of other NO_2 and NO molecules. N_2O_4 also forms from NO and O_2 molecules. Both N_2O_3 and N_2O_4 promote EEMPA fixation. N_2O_4 formation induced by O_2 is found to degrade the solvent the most. Lastly,

the anionic fixation mechanism of EEMPA is unlikely due to the formation of the unstable R_2N-anion.

Solvent density computed by CMD over a wide range of temperatures from 290 K to 370 K is slightly overestimated by less than 5%, compared to experiment. In the condensed phase, NO_2 forms N_2O_4 before interacting with EEMPA. AIMD simulations also show that NO_2 binds to the solvent, deprotonating EEMPA and forming HONO species with a second NO_2. Our simulations suggest two-step reaction involving the formation of a R_2N^* radical.

The calculated energy for the reaction of EEMPA with N_xO_y intermediates is small (from ~0.0 to less than about 0.5 eV, Figure 1). Such weak interactions suggest that the formation of nitramine/nitrosamine may be reversible process, further suggesting that EEMPA could be recovered under thermal stripping conditions. It is known that aqueous amines solvents are prone to oxidative degradation. Our study shows that the EEMPA water-lean solvent may have improved lifetime, but more importantly the potential to thermally decompose nitrosamines may provide sizable environmental benefits as well. Experimental studies are currently underway in our laboratory to examine this prediction.

In summary, we postulate that EEMPA fixation due to the presence of NO_x species during CO_2 capture follows a radical mechanism. This mechanistic understanding of solvent fixation can enable the design of new or modification of known CO_2 capture units where the presence of certain species, O_2 and NO_2, is minimized before interacting with the solvent. Ultimately, this is a step towards the rational design of carbon capture processes by increasing the lifetime of the solvent.

ASSOCIATED CONTENT

Supporting Information. Solvent density data.

AUTHOR INFORMATION

Corresponding Author

*Email: manhthuong.nguyen@pnnl.gov

Author Contributions

The manuscript was written through contributions of all authors. All authors have given approval to the final version of the manuscript.

Funding Sources

U.S. Department of Energy

ACKNOWLEDGMENT

This work was supported by the U.S. Department of Energy, Office of Fossil Energy, FWP 77217 (managed by National Energy Technology Laboratory). M.-T.N was also supported by the U.S. Department of Energy (DOE), Office of Science, Office of Basic Energy Sciences, Chemical Sciences, Geosciences, and Biosciences Division, project 81462 (Harnessing Confinement Effects, Stimuli, and Reactive Intermediates in Separations). PNNL is operated by Battelle for the US Department of Energy under Contract DE-AC05-76RL01830. This research used resources of the National Energy Research Scientific Computing Center (NERSC), a U.S. Department of Energy Office of Science User Facility located at Lawrence Berkeley National Laboratory, operated under Contract No. DE-AC02-05CH11231.

REFERENCES

(1) Hoegh-Guldberg, O.; Jacob, D.; Taylor, M.; Guillén Bolaños, T.; Bindi, M.; Brown, S.; Camilloni, I. A.; Diedhiou, A.; Djalante, R.; Ebi, K.; et al. The human imperative of stabilizing global climate change at 1.5°C. *Science* **2019**, *365* (6459). DOI: 10.1126/science.aaw6974.
(2) Kollias, L.; Zhang, D.; Allec, S. I.; Nguyen, M.-T.; Lee, M.-S.; Cantu, D. C.; Rousseau, R.; Glezakou, V.-A. Advanced Theory and Simulation to Guide the Development of CO2 Capture Solvents. *ACS Omega* **2022**, *7* (15), 12453-12466. DOI: 10.1021/acsomega.1c07398.
(3) Heldebrant, D. J.; Koech, P. K.; Glezakou, V.-A.; Rousseau, R.; Malhotra, D.; Cantu, D. C. Water-Lean Solvents for Post-Combustion CO2 Capture: Fundamentals, Uncertainties, Opportunities, and Outlook. *Chemical Reviews* **2017**, *117* (14), 9594-9624. DOI: 10.1021/acs.chemrev.6b00768.
(4) Li, J.; Li, Y.; Li, C.; Tu, R.; Xie, P.; He, Y.; Shi, Y. CO2 absorption and microwave regeneration with high-concentration TETA nonaqueous absorbents. *Greenhouse Gases: Science and Technology* **2022**. DOI: 10.1002/ghg.2148. Heldebrant, D. J.; Jiang, Y.; Zheng, R.; Barpaga, D.; Freeman, C.; Koech, P. K.; Malhotra, D.; Whyatt, G.; Zwoster, A. Performance and cost predictions of 2-EEMPA, and future opportunities for water-lean post-combustion capture solvents. *SSRN Electronic Journal* **2021**. DOI: 10.2139/ssrn.3813876.
(5) Azzi, M.; White, S. Emissions from amine-based post-combustion CO2 capture plants. In *Absorption-Based Post-combustion Capture of Carbon Dioxide*, 2016; pp 487-504.
(6) Rezaei, F.; Rownaghi, A. A.; Monjezi, S.; Lively, R. P.; Jones, C. W. SOx/NOx Removal from Flue Gas Streams by Solid Adsorbents: A Review of Current Challenges and Future Directions. *Energy & Fuels* **2015**, *29* (9), 5467-5486. DOI: 10.1021/acs.energyfuels.5b01286.
(7) Huang, Q.; Thompson, J.; Bhatnagar, S.; Chandan, P.; Remias, J. E.; Selegue, J. P.; Liu, K. Impact of Flue Gas Contaminants on Monoethanolamine Thermal Degradation. *Industrial & Engineering Chemistry Research* **2013**, *53* (2), 553-563. DOI: 10.1021/ie403426c.
(8) Dutcher, B.; Fan, M.; Russell, A. G. Amine-Based CO2 Capture Technology Development from the Beginning of 2013—A Review. *ACS Applied Materials & Interfaces* **2015**, *7* (4), 2137-2148. DOI: 10.1021/am507465f.
(9) Goff, G. S.; Rochelle, G. T. Monoethanolamine Degradation: O2 Mass Transfer Effects under CO2 Capture Conditions. *Industrial & Engineering Chemistry Research* **2004**, *43* (20), 6400-6408. DOI: 10.1021/ie0400245.
(10) da Silva, E. F.; Booth, A. M. Emissions from Postcombustion CO2 Capture Plants. *Environmental Science & Technology* **2013**, *47* (2), 659-660. DOI: 10.1021/es305111u.
(11) Sexton, A.; Dombrowski, K.; Nielsen, P.; Rochelle, G.; Fisher, K.; Youngerman, J.; Chen, E.; Singh, P.; Davison, J. Evaluation of Reclaimer Sludge Disposal from Post-combustion CO2 Capture. *Energy Procedia* **2014**, *63*, 926-939. DOI: 10.1016/j.egypro.2014.11.102.
(12) Lepaumier, H.; Picq, D.; Carrette, P.-L. New Amines for CO2 Capture. II. Oxidative Degradation Mechanisms. *Industrial & Engineering Chemistry Research* **2009**, *48* (20), 9068-9075. DOI: 10.1021/ie9004749.
(13) Karl, M.; Svendby, T.; Walker, S. E.; Velken, A. S.; Castell, N.; Solberg, S. Modelling atmospheric oxidation of 2-aminoethanol (MEA) emitted from post-combustion capture using WRF–Chem. *Science of The Total Environment* **2015**, *527-528*, 185-202. DOI: 10.1016/j.scitotenv.2015.04.108.
(14) Reynolds, A. J.; Verheyen, T. V.; Meuleman, E. Degradation of amine-based solvents. In *Absorption-Based Post-combustion Capture of Carbon Dioxide*, 2016; pp 399-423.

(15) Meuleman, E.; Cottrell, A.; Ghayur, A. Treatment of flue-gas impurities for liquid absorbent-based post-combustion CO2 capture processes. In *Absorption-Based Post-combustion Capture of Carbon Dioxide*, 2016; pp 519-551.
(16) Hamdy, L. B.; Goel, C.; Rudd, J. A.; Barron, A. R.; Andreoli, E. The application of amine-based materials for carbon capture and utilisation: an overarching view. *Materials Advances* **2021**, *2* (18), 5843-5880. DOI: 10.1039/d1ma00360g.
(17) Jahandar Lashaki, M.; Khiavi, S.; Sayari, A. Stability of amine-functionalized CO2 adsorbents: a multifaceted puzzle. *Chemical Society Reviews* **2019**, *48* (12), 3320-3405. DOI: 10.1039/c8cs00877a.
(18) Dumée, L.; Scholes, C.; Stevens, G.; Kentish, S. Purification of aqueous amine solvents used in post combustion CO2 capture: A review. *International Journal of Greenhouse Gas Control* **2012**, *10*, 443-455. DOI: 10.1016/j.ijggc.2012.07.005.
(19) Rezaei, F.; Jones, C. W. Stability of Supported Amine Adsorbents to SO2 and NOx in Postcombustion CO2 Capture. 2. Multicomponent Adsorption. *Industrial & Engineering Chemistry Research* **2014**, *53* (30), 12103-12110. DOI: 10.1021/ie502024z.
(20) Dai, N.; Mitch, W. A. Effects of Flue Gas Compositions on Nitrosamine and Nitramine Formation in Postcombustion CO2 Capture Systems. *Environmental Science & Technology* **2014**, *48* (13), 7519-7526. DOI: 10.1021/es501864a.
(21) Dai, N.; Mitch, W. A. Influence of Amine Structural Characteristics on N-Nitrosamine Formation Potential Relevant to Postcombustion CO2 Capture Systems. *Environmental Science & Technology* **2013**, *47* (22), 13175-13183. DOI: 10.1021/es4035396.
(22) Fostås, B.; Gangstad, A.; Nenseter, B.; Pedersen, S.; Sjøvoll, M.; Sørensen, A. L. Effects of NOx in the flue gas degradation of MEA. *Energy Procedia* **2011**, *4*, 1566-1573. DOI: 10.1016/j.egypro.2011.02.026.
(23) Voice, A. K.; Hill, A.; Fine, N. A.; Rochelle, G. T. Nitrosamine formation and mitigation in blended amines for CO2 capture. *International Journal of Greenhouse Gas Control* **2015**, *39*, 329-334. DOI: 10.1016/j.ijggc.2015.05.030.
(24) Yu, K.; Mitch, W. A.; Dai, N. Nitrosamines and Nitramines in Amine-Based Carbon Dioxide Capture Systems: Fundamentals, Engineering Implications, and Knowledge Gaps. *Environmental Science & Technology* **2017**, *51* (20), 11522-11536. DOI: 10.1021/acs.est.7b02597.
(25) Sun, Z.; Liu, Y. D.; Zhong, R. G. Carbon Dioxide in the Nitrosation of Amine: Catalyst or Inhibitor? *The Journal of Physical Chemistry A* **2011**, *115* (26), 7753-7764. DOI: 10.1021/jp202002m. Lv, C. L.; Liu, Y. D.; Zhong, R.; Wang, Y. Theoretical studies on the formation of N-nitrosodimethylamine. *Journal of Molecular Structure: THEOCHEM* **2007**, *802* (1-3), 1-6. DOI: 10.1016/j.theochem.2006.08.045.
(26) Shah, A. D.; Dai, N.; Mitch, W. A. Application of Ultraviolet, Ozone, and Advanced Oxidation Treatments to Washwaters To Destroy Nitrosamines, Nitramines, Amines, and Aldehydes Formed during Amine-Based Carbon Capture. *Environmental Science & Technology* **2013**, *47* (6), 2799-2808. DOI: 10.1021/es304893m.
(27) Chandan, P. A.; Remias, J. E.; Neathery, J. K.; Liu, K. Morpholine Nitrosation To Better Understand Potential Solvent Based CO2 Capture Process Reactions. *Environmental Science & Technology* **2013**, *47* (10), 5481-5487. DOI: 10.1021/es4003108.
(28) Fine, N. A.; Rochelle, G. T. Absorption of Nitrogen Oxides in Aqueous Amines. *Energy Procedia* **2014**, *63*, 830-847. DOI: 10.1016/j.egypro.2014.11.094.

(29) Wang, Z.; Zhang, Z.; Mitch, W. A. Role of absorber and desorber units and operational conditions for N-nitrosamine formation during amine-based carbon capture. *Water Research* **2020**, *170*. DOI: 10.1016/j.watres.2019.115299.
(30) Zhao, Y.-L.; Garrison, S. L.; Gonzalez, C.; Thweatt, W. D.; Marquez, M. N-Nitrosation of Amines by NO2 and NO: A Theoretical Study. *The Journal of Physical Chemistry A* **2007**, *111* (11), 2200-2205. DOI: 10.1021/jp0677703.
(31) Sun, Z.; Liu, Y. D.; Zhong, R. Theoretical investigation of reactivities of amines in the N-nitrosation reactions by N2O3. *Journal of Molecular Modeling* **2010**, *17* (4), 669-680. DOI: 10.1007/s00894-010-0750-4.
(32) Liu, Y.; Liu, Y.; Zhong, R.; Peng, B.; Schaefer, I. H. F. Effects of heavy metal ions on N-nitrosodimethylamine (NDMA) formation. *RSC Advances* **2016**, *6* (74), 70474-70479. DOI: 10.1039/c6ra11481d.
(33) Liu, C.; Liang, Z.; Yang, C.; Cui, F.; Zhao, Z. Nitrite-enhanced N-nitrosamines formation during the simulated tetracycline polluted groundwater chlorination: Experimental and theoretical investigation. *Chemical Engineering Journal* **2022**, *431*. DOI: 10.1016/j.cej.2021.133363.
(34) Lv, C. L.; Liu, Y. D.; Zhong, R. Theoretical Investigation of Nitration and Nitrosation of Dimethylamine by N2O4. *The Journal of Physical Chemistry A* **2008**, *112* (30), 7098-7105. DOI: 10.1021/jp8029924.
(35) Lv, C.-L.; Liu, Y. D.; Zhong, R.-g. Theoretical Investigation of N-Nitrosodimethylamine Formation from Dimethylamine Nitrosation Catalyzed by Carbonyl Compounds. *The Journal of Physical Chemistry A* **2009**, *113* (4), 713-718. DOI: 10.1021/jp8061674.
(36) Tang, Y.; Nielsen, C. J. Theoretical Study on the Formation and Photolysis of Nitrosamines (CH3CH2NHNO and (CH3CH2)2NNO) under Atmospheric Conditions. *The Journal of Physical Chemistry A* **2012**, *117* (1), 126-132. DOI: 10.1021/jp307812m.
(37) Chen, T.; Ge, Y.; Liu, Y.; He, H. N-nitration of secondary aliphatic amines in the particle phase. *Chemosphere* **2022**, *293*, 133639. DOI: 10.1016/j.chemosphere.2022.133639.
(38) Yu, Q.; Wang, P.; Ma, F.; Xie, H.-B.; He, N.; Chen, J. Computational investigation of the nitrosation mechanism of piperazine in CO2 capture. *Chemosphere* **2017**, *186*, 341-349. DOI: 10.1016/j.chemosphere.2017.07.114.
(39) Cantu, D. C.; Malhotra, D.; Nguyen, M. T.; Koech, P. K.; Zhang, D.; Glezakou, V. A.; Rousseau, R.; Page, J.; Zheng, R.; Perry, R. J. Molecular-Level Overhaul of γ-Aminopropyl Aminosilicone/Triethylene Glycol Post-Combustion CO2-Capture Solvents. *ChemSusChem* **2020**, *13* (13), 3429-3438.
(40) Jiang, Y.; Mathias, P. M.; Zheng, R. F.; Freeman, C. J.; Barpaga, D.; Malhotra, D.; Koech, P. K.; Zwoster, A.; Heldebrant, D. J. Energy-effective and low-cost carbon capture from point-sources enabled by water-lean solvents. *Journal of Cleaner Production* **2023**, *388*, 135696. DOI: 10.1016/j.jclepro.2022.135696.
(41) James III, R. E.; Keairns, D.; Turner, M.; Woods, M.; Kuehn, N.; Zoelle, A. *Cost and performance baseline for fossil energy plants volume 1: bituminous coal and natural gas to electricity*; National Energy Technology Laboratory (NETL), Pittsburgh, PA, Morgantown, WV …, 2019.
(42) Zheng, R. F.; Barpaga, D.; Mathias, P. M.; Malhotra, D.; Koech, P. K.; Jiang, Y.; Bhakta, M.; Lail, M.; V. Rayer, A.; Whyatt, G. A.; et al. A single-component water-lean post-combustion CO2 capture solvent with exceptionally low operational heat and total costs of capture –

comprehensive experimental and theoretical evaluation. *Energy & Environmental Science* **2020**, *13* (11), 4106-4113. DOI: 10.1039/d0ee02585b.
(43) Kothandaraman, J.; Saavedra Lopez, J.; Jiang, Y.; Walter, E. D.; Burton, S. D.; Dagle, R. A.; Heldebrant, D. J. Integrated Capture and Conversion of CO2 to Methane Using a Water-lean, Post-Combustion CO2 Capture Solvent. *ChemSusChem* **2021**, *14* (21), 4812-4819. DOI: 10.1002/cssc.202101590.
(44) Becke, A. D. Density-functional thermochemistry. III. The role of exact exchange. *The Journal of Chemical Physics* **1993**, *98* (7), 5648-5652. DOI: 10.1063/1.464913. Lee, C.; Yang, W.; Parr, R. G. Development of the Colle-Salvetti correlation-energy formula into a functional of the electron density. *Physical Review B* **1988**, *37* (2), 785-789. DOI: 10.1103/PhysRevB.37.785.
(45) Petersson, G. A.; Al-Laham, M. A. A complete basis set model chemistry. II. Open-shell systems and the total energies of the first-row atoms. *The Journal of Chemical Physics* **1991**, *94* (9), 6081-6090. DOI: 10.1063/1.460447. Petersson, G. A.; Bennett, A.; Tensfeldt, T. G.; Al-Laham, M. A.; Shirley, W. A.; Mantzaris, J. A complete basis set model chemistry. I. The total energies of closed-shell atoms and hydrides of the first-row elements. *The Journal of Chemical Physics* **1988**, *89* (4), 2193-2218. DOI: 10.1063/1.455064.
(46) Aprà, E.; Bylaska, E. J.; de Jong, W. A.; Govind, N.; Kowalski, K.; Straatsma, T. P.; Valiev, M.; van Dam, H. J. J.; Alexeev, Y.; Anchell, J.; et al. NWChem: Past, present, and future. *The Journal of Chemical Physics* **2020**, *152* (18). DOI: 10.1063/5.0004997.
(47) Hess, B.; Kutzner, C.; van der Spoel, D.; Lindahl, E. GROMACS 4: Algorithms for Highly Efficient, Load-Balanced, and Scalable Molecular Simulation. *Journal of Chemical Theory and Computation* **2008**, *4* (3), 435-447. DOI: 10.1021/ct700301q.
(48) Jorgensen, W. L.; Maxwell, D. S.; Tirado-Rives, J. Development and Testing of the OPLS All-Atom Force Field on Conformational Energetics and Properties of Organic Liquids. *Journal of the American Chemical Society* **1996**, *118* (45), 11225-11236. DOI: 10.1021/ja9621760.
(49) Dodda, L. S.; Cabeza de Vaca, I.; Tirado-Rives, J.; Jorgensen, W. L. LigParGen web server: an automatic OPLS-AA parameter generator for organic ligands. *Nucleic Acids Research* **2017**, *45* (W1), W331-W336. DOI: 10.1093/nar/gkx312. Dodda, L. S.; Vilseck, J. Z.; Tirado-Rives, J.; Jorgensen, W. L. 1.14*CM1A-LBCC: Localized Bond-Charge Corrected CM1A Charges for Condensed-Phase Simulations. *The Journal of Physical Chemistry B* **2017**, *121* (15), 3864-3870. DOI: 10.1021/acs.jpcb.7b00272. Jorgensen, W. L.; Tirado-Rives, J. Potential energy functions for atomic-level simulations of water and organic and biomolecular systems. *Proceedings of the National Academy of Sciences* **2005**, *102* (19), 6665-6670. DOI: 10.1073/pnas.0408037102.
(50) Bernetti, M.; Bussi, G. Pressure control using stochastic cell rescaling. *The Journal of Chemical Physics* **2020**, *153* (11), 114107.
(51) Perdew, J. P.; Burke, K.; Ernzerhof, M. Generalized Gradient Approximation Made Simple. *Physical Review Letters* **1996**, *77* (18), 3865-3868. DOI: 10.1103/PhysRevLett.77.3865. Grimme, S.; Antony, J.; Ehrlich, S.; Krieg, H. A consistent and accurate ab initio parametrization of density functional dispersion correction (DFT-D) for the 94 elements H-Pu. *The Journal of Chemical Physics* **2010**, *132* (15). DOI: 10.1063/1.3382344.
(52) Lippert, G.; Hutter, J.; Parrinello, M. A hybrid Gaussian and plane wave density functional scheme. *Molecular Physics* **1997**, *92* (3), 477-488. DOI: 10.1080/002689797170220.
(53) VandeVondele, J.; Hutter, J. Gaussian basis sets for accurate calculations on molecular systems in gas and condensed phases. *The Journal of chemical physics* **2007**, *127* (11), 114105. DOI: 10.1063/1.2770708.

(54) Evans, D. J.; Holian, B. L. The nose–hoover thermostat. *The Journal of chemical physics* **1985**, *83* (8), 4069-4074. DOI: 10.1063/1.449071.
(55) Kühne, T. D.; Iannuzzi, M.; Del Ben, M.; Rybkin, V. V.; Seewald, P.; Stein, F.; Laino, T.; Khaliullin, R. Z.; Schütt, O.; Schiffmann, F.; et al. CP2K: An electronic structure and molecular dynamics software package - Quickstep: Efficient and accurate electronic structure calculations. *The Journal of Chemical Physics* **2020**, *152* (19). DOI: 10.1063/5.0007045.
(56) Henkelman, G.; Uberuaga, B. P.; Jónsson, H. A climbing image nudged elastic band method for finding saddle points and minimum energy paths. *The Journal of chemical physics* **2000**, *113* (22), 9901-9904.
(57) Tang, W.; Sanville, E.; Henkelman, G. A grid-based Bader analysis algorithm without lattice bias. *Journal of Physics: Condensed Matter* **2009**, *21* (8), 084204.
(58) Dai, N.; Shah, A. D.; Hu, L.; Plewa, M. J.; McKague, B.; Mitch, W. A. Measurement of Nitrosamine and Nitramine Formation from NOx Reactions with Amines during Amine-Based Carbon Dioxide Capture for Postcombustion Carbon Sequestration. *Environmental Science & Technology* **2012**, *46* (17), 9793-9801. DOI: 10.1021/es301867b.
(59) Gadzhiev, O. B.; Ignatov, S. K.; Gangopadhyay, S.; Masunov, A. E.; Petrov, A. I. Mechanism of nitric oxide oxidation reaction (2NO+ O2→ 2NO2) revisited. *Journal of Chemical Theory and Computation* **2011**, *7* (7), 2021-2024.
(60) Glendening, E. D.; Halpern, A. M. Ab initio calculations of nitrogen oxide reactions: Formation of N2O2, N2O3, N2O4, N2O5, and N4O2 from NO, NO2, NO3, and N2O. *The Journal of chemical physics* **2007**, *127* (16), 164307. DOI: 10.1063/1.2777145.
(61) Oyamada, R. Phase Diagrams of ThCl4 Systems Containing NaCl, KCl and LiCl and the Limitation of the Congruently Melting Compounds Formation. *Denki Kagaku oyobi Kogyo Butsuri Kagaku* **1971**, *39* (1), 2-5. DOI: 10.5796/kogyobutsurikagaku.39.2.
(62) Rezaei, F.; Jones, C. W. Stability of Supported Amine Adsorbents to SO2 and NOx in Postcombustion CO2 Capture. 1. Single-Component Adsorption. *Industrial & Engineering Chemistry Research* **2013**, *52* (34), 12192-12201. DOI: 10.1021/ie4019116.
(63) Cantu, D. C.; Lee, J.; Lee, M.-S.; Heldebrant, D. J.; Koech, P. K.; Freeman, C. J.; Rousseau, R.; Glezakou, V.-A. Dynamic acid/base equilibrium in single component switchable ionic liquids and consequences on viscosity. *The Journal of Physical Chemistry Letters* **2016**, *7* (9), 1646-1652. DOI: 10.1021/acs.jpclett.6b00395.

TOC